# Laboratory simulations and parameterization of the primary marine aerosol production

E. M. Mårtensson and E. D. Nilsson
Department of Meteorology, Stockholm University, Stockholm, Sweden

G. de Leeuw and L. H. Cohen
Physics and Electronics Laboratory, Netherlands Organization for Applied Scientific Research, The Hague, Netherlands

H.-C. Hansson
Air Pollution Laboratory, Institute of Applied Environmental Research, Stockholm University, Stockholm, Sweden

Received 5 March 2002; revised 1 November 2002; accepted 10 February 2003; published 15 May 2003.

[1] A major source of the primary marine aerosol is the bursting of air bubbles produced by breaking waves. Several source parameterizations are available from the literature, usually limited to particles with a dry diameter $D_p > 1$ μm. The objective of this work is to extend the current knowledge to submicrometer particles. Bubbles were generated in synthetic seawater using a sintered glass filter, with a size spectra that are only partly the same spectra as measured in the field. Bubble spectra, and size distributions of the resulting aerosol (0.020–20.0 μm $D_p$) of the resulting aerosol, were measured for different salinity, water temperature ($T_w$), and bubble flux. The spectra show a minimum at ~1 μm $D_p$, which separates two modes, one at ~0.1 μm, with the largest number of particles, and one at 2.5 μm $D_p$. The modes show different behavior with the variation of salinity and water temperature. When the water temperature increases, the number concentration $N_p$ decreases for $D_p < 0.07$ μm, whereas for $D_p > 0.35$ μm, $N_p$ increases. The salinity effect suggests different droplet formation processes for droplets smaller and larger than 0.2 μm $D_p$. The number of particles produced per size increment, time unit, and whitecap surface ($\Phi$) is described as a linear function of $T_w$ and a polynomial function of $D_p$. Combining $\Phi$ with the whitecap coverage fraction $W$ (in percent), an expression results for the primary marine aerosol source flux $dF_0/d\log D_p = W\,\Phi$ ($m^{-2}\ s^{-1}$). The results are compared with other commonly used formulations as well as with recent field observations. Implications for aerosol-induced effects on climate are discussed. *INDEX TERMS:* 0305 Atmospheric Composition and Structure: Aerosols and particles (0345, 4801); 0312 Atmospheric Composition and Structure: Air/sea constituent fluxes (3339, 4504); 0322 Atmospheric Composition and Structure: Constituent sources and sinks; *KEYWORDS:* primary aerosol, marine aerosol, sea salt, air-sea exchange, bubble bursting

**Citation:** Mårtensson, E. M., E. D. Nilsson, G. de Leeuw, L. H. Cohen, and H.-C. Hansson, Laboratory simulations and parameterization of the primary marine aerosol production, *J. Geophys. Res.*, *108*(D9), 4297, doi:10.1029/2002JD002263, 2003.

## 1. Introduction

[2] Already *Aitken* [1881] suggested that the oceans are a source for sea-salt aerosol particles. The primary marine aerosol is emitted from the water surface into the atmosphere directly as droplets with the composition of seawater enriched with chemical compounds, bacteria and viruses occurring in the upper water column and in the film covering the water surface. A major source of the primary marine aerosol is the bursting of air bubbles produced by breaking waves [e.g., *Blanchard*, 1963, 1983]. In wind speeds higher than about 9 m $s^{-1}$, spume drops are produced by direct tearing from the wave crests [*Monahan et al.*, 1983]. The surface manifestation of a breaking wave is a whitecap. Relationships between the concentrations of airborne sea-salt aerosol mass and whitecap cover and/or wind speed were already discovered in the 1950s [*Woodcock*, 1953]. On average, globally about 1% of the oceans is covered with whitecaps.

[3] It is generally assumed that the bursting of bubbles produces two types of droplets; film drops ejected from the rim of the receding film cap when the bubble film opens [*Spiel*, 1998] and jet drops formed from the break up of the vertically rising jet of water from the collapsing bubble cavity [e.g., *Blanchard and Woodcock*, 1957]. The number of film and jet drops produced depends on the size of the bubble [e.g., *Blanchard*, 1963; *Blanchard and Syzdek*, 1988]: Small bubbles produce only jet drops; large bubbles produce only film drops. The size of the jet drops is about


0148-0227/03/2002JD002263

1/10 of the parent bubble diameter size $D_b$ [*Blanchard*, 1963; *Spiel* 1994], which places the jet drops in the supermicrometer aerosol size range. *Spiel* [1997a] deduced that a maximum number of six jet droplets can be produced and that bubbles larger than 3.4 mm $D_b$ produce no jet drops. It is believed that film drops would dominate in the submicrometer aerosol [e.g., *Woolf et al.*, 1987] and that they can be up to several hundred per bubble and increase in number with $D_b$ [*Blanchard*, 1963]. Studies by *Resch and Afeti* [1992] suggest that for bubbles >2 mm, film drops dominate in number over jet drops, and *Spiel* [1998] concluded that bubbles smaller than ~2 mm do not form any film drops.

[4] When *Cipriano et al.* [1987] made laboratory experiments, they measured the flux of particles per whitecap area ($F_p$) and found that most of the particles where submicron. *Blanchard and Syzdek* [1988] and *Resch and Afeti* [1992] made experiments with single bubbles and found a maximum in the numbers of particles produced for bubbles with 2–2.5 mm and 2.14 mm $D_b$, respectively. A majority of these particles had a dry diameter $D_p$ from 0.056 to 0.300 μm [*Resch and Afeti*, 1992]. This was the first size resolved distribution of the submicron sea-salt particles but only for a very specific bubble size. A hypothesis to explain these observations was based on photographic evidence by *Spiel* [1997b], and in a theoretical model, *Spiel* [1998] proposed that the film of bubbles with diameter <3 mm rolls up instead of disintegrating, with a rim with an irregular structure with mass density fluctuations. The areas with large mass attain a higher momentum until they are ejected at very high velocity in a near-horizontal direction. This process may still form particles, but not from the disintegration of the film, perhaps by splashing or through the formation of the small secondary bubbles observed by *Leifer et al.* [2000] and their subsequent collapse and ejection of jet drops.

[5] Field experiments at sea show a large contribution of primary marine aerosols in the submicrometer aerosol size range. For example, *O'Dowd and Smith* [1993] observed number distributions with two modes: a jet drop mode with a dry median diameter of 2 μm and a film drop mode with a dry median diameter of 0.2 μm. The number concentrations increased exponentially with the wind speed. *Nilsson et al.* [2001] measured directly the primary marine aerosol flux using the eddy covariance method. The measured aerosol number flux $F_0$ increased exponentially with the wind speed:

$$F_0 = 10^{0.20\overline{U}_{10}-1.71}\left(10^6\ \mathrm{m^{-2}s^{-1}}\right) \quad 3 < U_{10} < 14\ \mathrm{m\ s^{-1}} D_p > 0.01\mu\mathrm{m} \tag{1}$$

where $\overline{U}_{10}$ is the mean wind speed at 10 m above sea level. The flux appeared to be dominated by two modes centered at about 0.1 μm and 1 μm $D_p$, respectively. Assuming that the aerosol is sea salt, the smallest of the modes observed by *O'Dowd et al.* [1997] and *Nilsson et al.* [2001] correspond to a wet diameter of a few hundred nanometers. Earlier insights suggest that droplets in this size range must be either film drops from bubbles of a few millimeters in diameter or jet drops from bubbles of a few micrometers in diameter. The latter is unrealistic since such small bubbles would readily dissolve in the water. An alternative explanation [*Spiel*, 1998] might be that they are produced by splashes of larger film drops ejected at a downward angle.

[6] Several parameterizations for the sea spray generation function $dF/dr_0$ (number of droplets produced per square meter of surface per second per micrometer radius increment), where $r_0$ is the radius of a droplet at formation, are available in literature (see *Andreas* [1998] for an overview). A commonly used formulation for the source function [*Monahan et al.*, 1986] is based on laboratory observations of $dF/dr_0$ and empirical relations for the whitecap cover ($W$ in percent) as a function of the wind speed [*Monahan and O'Muircheartaigh*, 1980]:

$$W = 3.84 \times 10^{-4} U_{10}^{3.41} \tag{2}$$

where $U_{10}$ is the wind speed at 10 m above the sea surface. Thus the source function for bubble-mediated sea spray is highly nonlinearly dependent on the surface wind (or friction velocity). The whitecap coverage has been shown to vary with temperature [*Bortkovskii*, 1983], but no parameterization including this variation is available. Other parameterizations are based on considerations of the balance between production and removal [e.g., *Smith et al.*, 1993]. The summary of *Andreas* [1998] of sea spray source functions shows differences of up to 8 decades, but parameterizations that are currently used for various applications show better agreement (a few orders of magnitude differences). An important limitation of the present parameterizations is that they are confined to particles >0.5 μm $D_p$, in most cases >1 μm $D_p$, although they are sometimes extrapolated to smaller sizes. Studies presented by *de Leeuw et al.* [2000] show that the source function of *Monahan et al.* [1986] applies best to particles with diameters <10 μm at formation, whereas the formulation offered by *Smith et al.* [1993] gives better results for larger particles.

[7] The objective of this work is to extend current knowledge on sea-salt aerosol production to smaller particles to better understand recent field observations [*O'Dowd and Smith*, 1993; *Nilsson et al.*, 2001] and their implications, for example, for climate and various processes involving sea-salt aerosol. As discussed above, while submicrometer sized primary marine aerosol particles have been observed in the field, they have not been observed during laboratory studies, with state of the art aerosol equipment. In view of the uncertainty regarding the discrimination between film and jet drops during experiments, in the presented analysis no distinction will be made.

## 2. Experiment

[8] To achieve this objective, experiments were made in a closed chamber from which all aerosols had been effectively removed before the start of each experiment. Bubbles were generated in water with different salinities and temperatures by pumping filtered air through a submerged sintered glass filter. The size distributions of the bubbles and the aerosols produced from them were measured. The experimental setup, the equipment used, and the experimental procedures are described in sections 2.1–2.3.

### 2.1. Bubble Chamber

[9] The experimental setup (Figure 1a) consisted of a flask with a volume of 2.0 L and with three necks of which one was plugged (the plugged neck is not included in

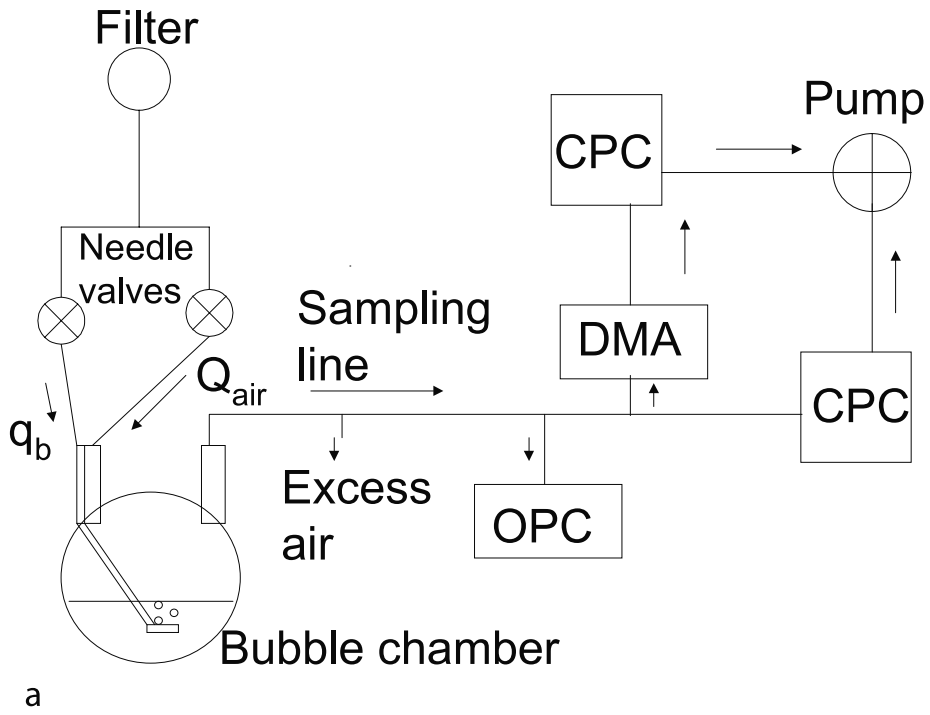


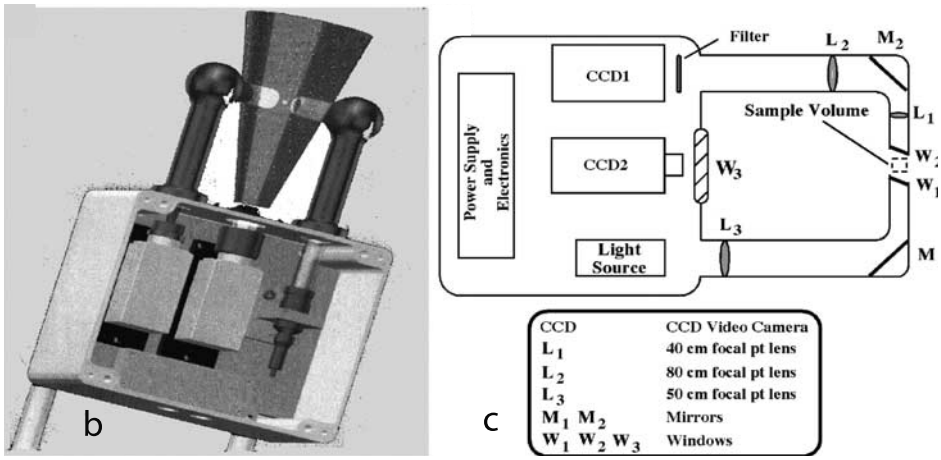


**Figure 1.** (a) Experimental setup with the bubble chamber and sampling system. (b) TNO-FEL mini bubble measuring system (MiniBMS). The sample volume is determined by the distance between the tubes and the width of the laser beam. The sample volume is inside the conical field of view of the overview camera. (c) MiniBMS block schematic with key.

Figure 1). The flask was filled with 1.0 L of water. A sintered glass filter with pore sizes of 20–40 μm was inserted through one neck. The filter was situated about 4 cm below the water surface. Filtered air was forced through the glass filter to generate bubbles. The airflow ($q_b$) was controlled by a needle valve. Aerosols produced from these bubbles were sampled in air expelled through the opposite neck. To provide sufficient airflow, filtered air ($Q_{\text{air}}$) was pumped into the flask through a second inlet, at a rate of 3.6 L min$^{-1}$. The aerosol in the flask was sampled with a flow of 3.0 L min$^{-1}$; an opening in the sampling line was used as an outlet for the excess air (0.6 L min$^{-1}$). Prior to each experiment, the chamber was flushed with filtered air and with $q_b$ = 0.0 L min$^{-1}$ for ~5–10 min until no particles were detected. Subsequently, $q_b$ was set to a constant value, and the aerosol concentrations were monitored. After an initial rise in the concentrations a steady state was reached in which the bubble-mediated aerosol production was in balance with the removal (after 5 min). Then the particle size distributions were measured during 30 min.

[10] The experiments were undertaken using water with three different salinities ($S_w$): 0.0‰, 9.2‰, representative of the surface water in the south of the Baltic Sea, and 33‰, which is more representative of the ocean. To achieve this,

pure Milli-Q water was used ($S_w$ = 0.0‰), in which synthetic sea salt (Tropic Marin, manufactured for saltwater aquariums and containing all the major sea-salt components in proportions close to that found in the ocean) was dissolved. The salinity was measured with an Aanderaa salinometer. The first measurements were made at the laboratory ambient temperature of 23°C, but in most of the measurements we used a cooler (MGW Lauda RM20, accuracy ± 0.1°) to set the water temperatures to −2°, 5°, 15°, and 25°C.

### 2.2. Bubble Spectra

[11] Bubble size distributions were measured with the TNO Mini-Bubble Measuring System (Mini-BMS) (Figures 1b and 1c), described in detail by *Leifer et al.* [2002]. Briefly, the Mini-BMS consists of a light source (a light-emitting diode, wavelength 880 nm) and optics components to illuminate the sample volume that is monitored by a video camera through a telescope. Light source and video camera are contained together in a box equipped with two conical tubes containing mirrors and lenses to guide the light beam through an open sample volume, which is constrained, by the windows at the end of the conical tubes. The length of the sample volume is 20 mm, and the volume is 0.11 $mm^3$. The video signals are fed into a VHS video recorder and are analyzed afterward using a frame grabber and a dedicated image-processing package.

[12] The Mini-BMS measures the bubble concentration from 30 to 1240 μm bubble diameters $D_b$ over 20 intervals. In the experiments, bubble sizes were determined by discriminating the bubble from the background via image thresholding [*Leifer et al.*, 2002]. In-focus bubbles are dark with a white center, surrounded by a faint reflective halo (from off-axis light from the background screen). Slightly out of focus bubbles also exhibit a glory without the central white spot. The appropriate threshold was determined during a series of calibration experiments described by I. Leifer et al. (Calibrating optical bubble size by the displaced mass method, submitted to *Chemical Engineering Science*, 2002). Because the measurement volume and the sampling time are known, conversion to a bubble concentration distribution is straightforward. Owing to the small sample volume, usually coincidence is no problem.

[13] The spectra of the bubbles generated by the sintered glass filter were measured in a small aquarium. The aerators were fed with air filtered using a Gelman 9967-008 filter with a 1 μm pore size. The airflow in the bubble generator was measured with a Brooks Instrument, ShoRate 1355/R-2-15-AAA/Saphire float, with an accuracy of 5%. Salinity, water temperature, and the depth at which the bubbles were generated were similar to those used in the aerosol measurements. Bubbles were measured with the Mini-BMS at 1 cm below the water surface, during 10 min.

### 2.3. Aerosol Spectra

[14] The size distribution of particles with dry diameters between 0.020 and 0.135 μm, distributed over 11 size channels, was measured with a differential mobility particle sizer (DMPS), consisting of a condensation particle counter model TSI 3010 and a differential mobility analyzer (DMA).

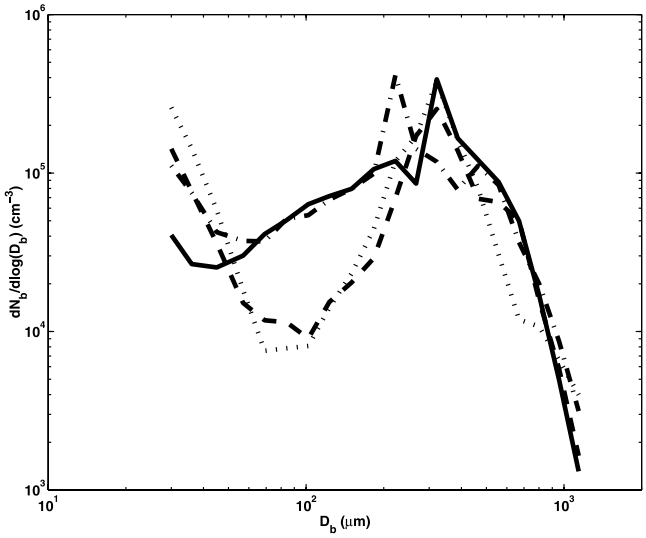


**Figure 2.** Spectra of bubbles generated by the sintered glass filter for −2°C (dotted line), 5°C (dashed line), 15°C (dot-dashed line), and 25°C (solid line). The flow $q_b$ through the glass filter was kept constant at 10 mL $min^{-1}$ and the salinity was 33.0‰.

[15] The aerosol particle size distributions with diameters between 0.135 μm and 20.0 μm, distributed over 30 size channels, were measured with an optical particle counter (OPC), a passive cavity aerosol spectrometer probe (PCASP-X) from particle measuring system (Boulder, Colorado, USA). The particles measured with the DMA and the PCASP-X were dry because they lost the associated water in the sampling tube where they were mixed with dry sheath air. When not explicitly specified, all aerosol particle diameters in this manuscript are for the dry aerosol.

## 3. Results

### 3.1. Bubble Spectra

[16] The bubble size distributions in Figure 2 exemplify the typical bubble size distribution for the four different temperatures used in our experiments, with a salinity of 33‰ and a flow rate of 10 mL $min^{-1}$. There was a bimodal distribution, with a rather sharp peak at 220 or 320 μm, a minimum around 100 μm or lower, and concentrations rising with bubble size decreasing toward the lowest observed bubble diameter. The water temperature, the flow rates, and salinity influenced the bubble concentration around 100 μm but had very little effect on the bubble concentrations at the lower extreme of the spectra and on bubbles >200−300 μm. In particular, for bubbles larger than ~350 μm the spectra are very similar in all conditions. In summary, the sintered glass filter does produce bubbles in the same size range as breaking waves in the real sea but only partly in the same spectra [*Medwin and Breitz*, 1989; *Bowyer*, 2001].

### 3.2. Aerosol Spectra

[17] The experiments were repeated for different bubble flow, temperature, and salinity. The aerosol spectra for different flow rates (10, 60, and 120 mL $min^{-1}$) all showed bimodal number concentration with a mode centered at

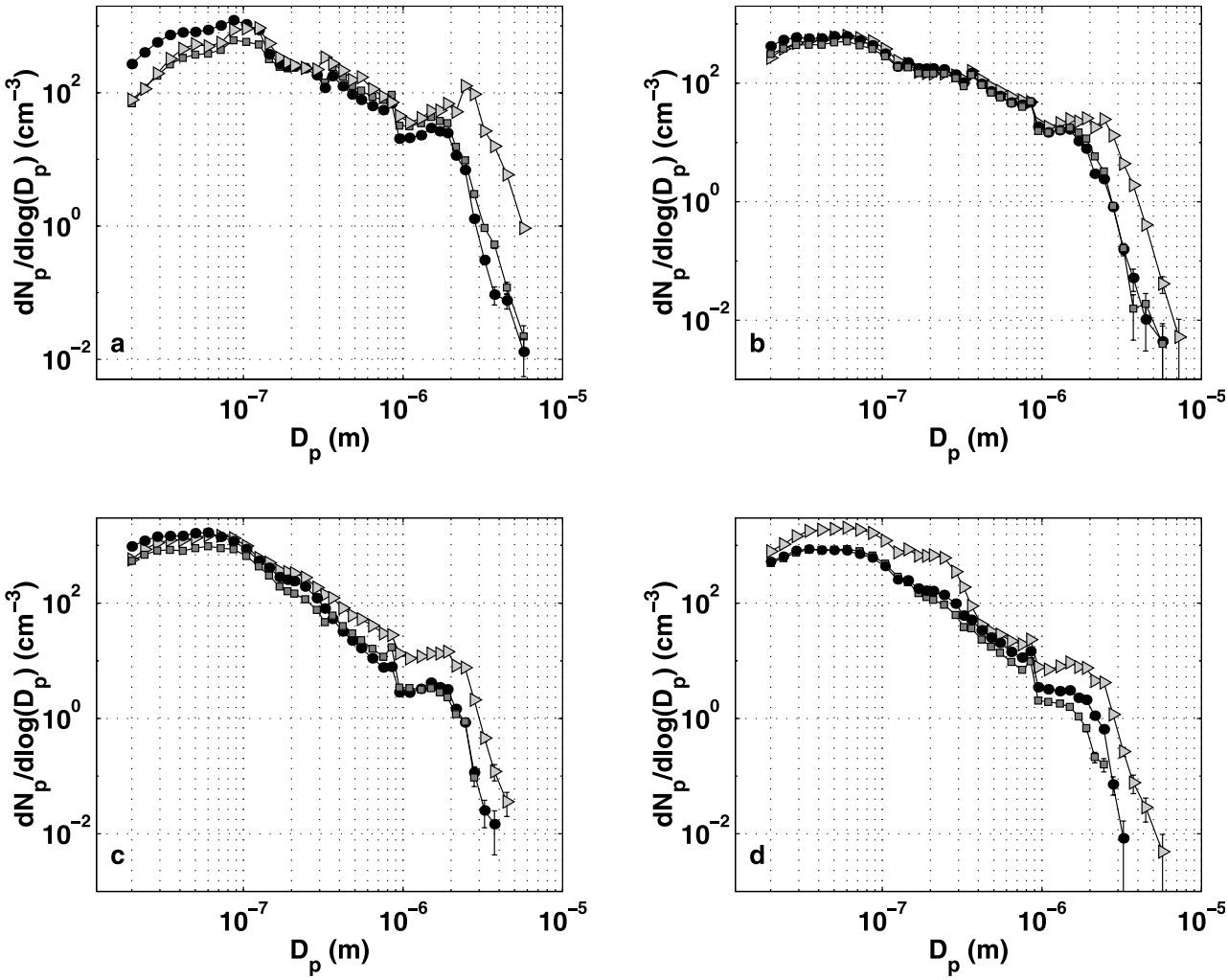


**Figure 3.** All data, two different experiments with a flow rate of 10 mL $min^{-1}$ (squares and dots) and one at 13 mL $min^{-1}$ (triangles), with a salinity of 33‰ and temperatures of (a) 25°C, (b) 15°C, (c) 5°C, and (d) −2°C.

~0.1 μm $D_p$ and another at 2–3 μm $D_p$. Since our lowest flow rate around 10 mL $min^{-1}$ appears to correspond most closely to real whitecap conditions, these are the experiments we will use from now on.

[18] Figure 3 includes all experiments at each temperature, two with the bubble flow rates of 10 mL $min^{-1}$ (squares and dots) and one at 13 mL $min^{-1}$ (triangles) with a salinity of 33‰. At $q_b$ = 13 mL $min^{-1}$ the number concentration is higher because then a larger area is covered with bubbles, especially for the larger particles. Each data point is marked, and all data points include the instrument error bar. It can be seen that the measurement error is small (smaller than the marker for the small sizes) except for the largest particles in the OPC range, because these were present in very small numbers.

[19] Figure 4a shows an example of the measured aerosol size distribution. Common features are the two modes with modal diameters around 0.05–0.1 μm and 2–3 μm $D_p$, respectively. This is qualitatively in agreement with *O'Dowd et al.* [1997], who found two modes at similar sizes and identified them as film and jet drop modes; see Figure 4d. Figure 4a also illustrates the typical measurement error bar for one 30 min experiment. This error is small because of the large number of particles counted at all sizes during 30 min except in the upper part of the OPC range. Figure 4b shows the variability in the aerosol size distribution within the 30 min period of measurements for the experiment. The standard deviation was very small in the submicrometer range but was larger in the supermicrometer range because of low counts. The Figure 4b demonstrates that both aerosol modes at ~100 nm and 2–3 μm $D_p$ are larger than the variation during the experiment. Figure 4c illustrates the reproducibility by showing the variation between three experiments made with the same conditions ($T_w$, $S_w$, and $q_b$). Using two different temperatures (5° and 25°C), Figure 4c demonstrates that the differences in the size distribution between these two temperatures are larger than ±1 standard deviation for particles smaller than ~80 nm dry diameter and for particles between 400 nm and 2 μm dry diameter. The variation between experiments at identical conditions is only larger than the average difference in the range where the average size distributions are crossing (80–400 nm) and in the uppermost OPC range where the relative errors are large because of very few particles. The reprodu-

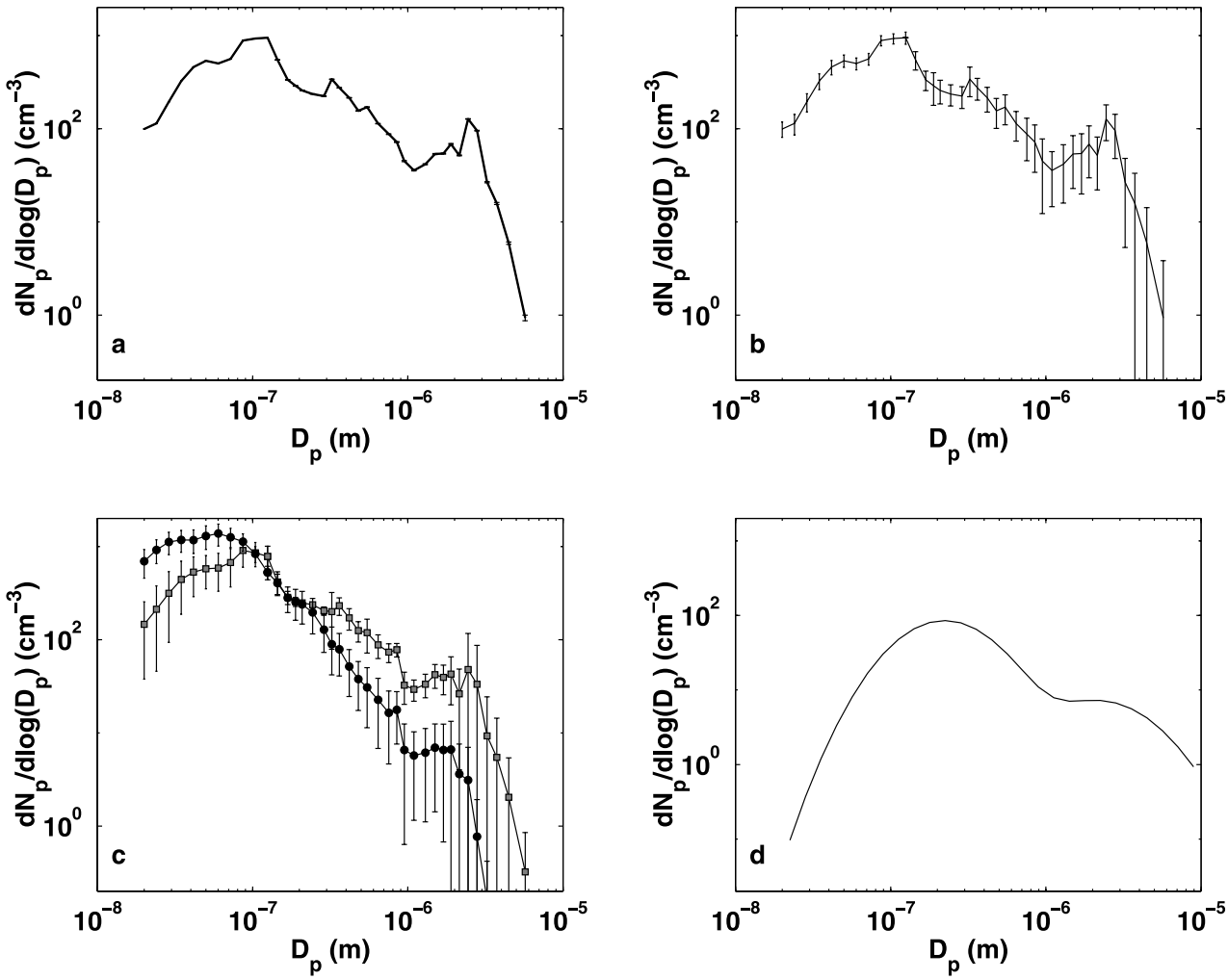


**Figure 4.** (a) The mean size distribution and measurement error bar for one 30 min experiment. (b) The mean and variability in the aerosol size distribution within the 30 min period of measurements for one of the experiment (±1 standard deviation). (c) The mean size distributions of several experiments made at the same conditions with the standard deviation between these experiments for two different temperatures. Dots represent 5°C, and squares represent 25°C. (d) Lognormal fit to measured sea-salt aerosol number concentration at a wind speed of 9 m $s^{-1}$ (parameterization from *O'Dowd et al.* [1997]).

cibility of the experiments was good, and the bimodal feature of the size distribution was always present.

### 3.2.1. Effects of Salinity

[20] Figure 5 illustrates the effects of the salinity on the dry aerosol number concentration ($N_p$ $cm^{-3}$), measured with $q_b$ = 13 mL $min^{-1}$ and $T_w$ = 23°C. Using Milli-Q water ($S_w$ = 0), there were only a small amount of particles, all with $D_p$ < 0.7 μm. For the aerosols generated by bubbles in the sea-salt solutions ($S_w$ = 9.2‰ and 33.0‰), two modes were observed. For the higher $S_w$ the small particle mode appears at ~0.1 μm $D_p$, whereas for the lower $S_w$ the small particle mode appears at a $D_p$ that is roughly a factor 1.5 smaller. This is in agreement with the expectation that for a similar drop size spectra at formation the less saline droplets produced at the lower salinity would evaporate to particles with smaller $D_p$. The ratio between the dry radius particles resulting from 33.0 and 9.2‰ salinity is $(33.0/9.2)^{1/3} \sim 1.5$. The total volume in the $D_p$ < 0.2 μm range varies approximately proportionally to the water salinity. In contrast, for $D_p$ > 0.2 μm (compare the peak at ~2 μm) the aerosol spectra have a similar shape for both salinities, but the concentrations are an order of magnitude different. This suggests that in the $D_p$ < 0.2 μm range, salinity does not affect the original droplet production, just the size of the residual dry aerosol, and that at formation, droplets have the salinity of seawater, as was also assumed by *Andreas* [1998]. However, for $D_p$ > 0.2 μm the ratio between the salinity and the volume of aerosol particles is larger for higher salinity, which suggests that the droplet formation is affected by the salinity. This indicates different droplet formation processes for particles with $D_p$ smaller than ~0.2 μm and for particles larger than this size.

### 3.2.2. Effects of Water Temperature

[21] In Figure 6, aerosol number size distributions are presented for four water temperatures. The flow was 13 mL $min^{-1}$ and $S_W$ was 33‰. For $D_p$ > 0.35 μm the number concentration increased with increasing temperature, and the shapes of the size distributions were similar at all

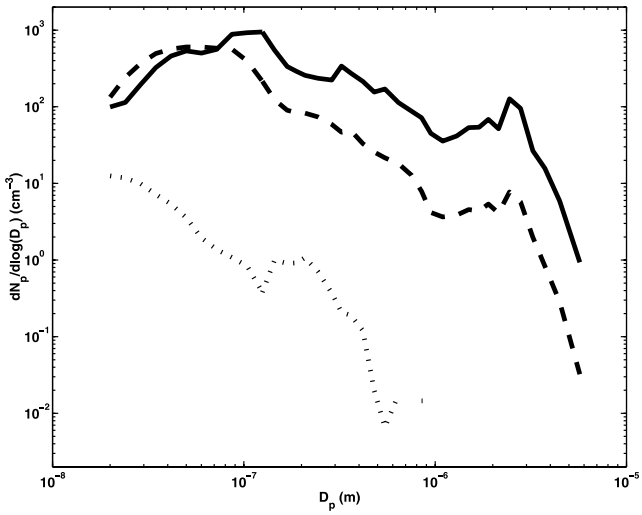


**Figure 5.** Number distributions of primary marine aerosols produced from bubbles in water with the salinity of 0.0‰ (dotted line), 9.2‰ (dashed line), and 33.0‰ (solid line). $T_w$ was 23°C, and $q_b$ was 13 mL min$^{-1}$.

temperatures. However, for $D_p < 0.07$ μm the number concentration decreased with increasing temperature. In a transition range $D_p = 0.07$ to 0.35 μm the curves cross, but there is no clear trend with the water temperature. Like for salinity, this indicates different droplet formation processes, in this case below and above 0.07–0.35 μm $D_p$.

## 4. Discussion

### 4.1. Parameterization

#### 4.1.1. Parameterization Approach

[22] The experimental data show that the number distributions of aerosols produced by bubble bursting depends on $S_w$, $q_b$, $T_w$, and $D_p$. Below a parameterization of the aerosol production will be derived for a salinity of 33‰, the value that approximately applies to most of the ocean, and $q_b \approx$ 10 mL min$^{-1}$, because most of the bubble spectra were measured at this flow and because the bubble concentration at this flow was most close to that observed in real whitecaps. A parameterization will be sought for the number of particles produced per second, logarithmic size increment, and water surface area with bubbles ($A_b$) (in m$^{-2}$, $A_b$ = 3.0172 × 10$^{-4}$ m$^{-2}$ for $q_b$ = 10 mL min$^{-1}$ and $A_b$ = 3.8013 × 10$^{-4}$ m$^{-2}$ for $q_b$ = 13 mL min$^{-1}$) for each temperature (in kelvins) and aerosol size interval ($j$ = 1–41):

$$\Phi_j = \frac{1}{A_b}\frac{dn_p^j}{d\,\log D_p} \tag{3}$$

where $n_p^j$ (s$^{-1}$) is the number of particles produced at the water surface in each size interval during a certain period of time, as measured with the DMPS and the OPC. In this parameterization we will use the units of meters, seconds, and kelvins.

#### 4.1.2. Temperature Dependency

[23] As shown in Figure 6, the number of particles produced depends on the water temperature and varies with the particle size. This is further illustrated in Figure 7 where $\Phi_j$ is plotted as a function of water temperature for two size ranges ($\Phi_4$, 0.0316–0.038 μm $D_p$, and $\Phi_{29}$, 1.4–1.6 μm $D_p$) for all the experiments at each temperature. The variation of the number particle production with the water temperature depends on the particle size: For example, $\Phi_4$ decreases with increasing temperature (Figure 7a), and $\Phi_{29}$ increases with increasing temperature (Figure 7b). A linear fit was made to the data in each DMPS and OPC size channel for $T_w$ = 271–298 K. Using these fits, $\Phi_j$ can now be written as

$$\Phi_j = a_j T_w + b_j \tag{4}$$

In equation (4), $T_w$ is expressed in kelvins. Qualitatively, the results presented in Figure 7 agree with those presented by *Bowyer et al.* [1990], who showed a large increase of small particles for $T_w < 20$°C and also an increase of the number concentration for larger particles with increasing water temperature. The differences in the bubble spectra, surface tension, viscosity, and density of the water at different temperatures are probably an important explanation of why the aerosol number concentration and size distribution depend on the water temperature. Another important factor that may influence the aerosol production is the degree of saturation of the water, as reported by, for example, *Blanchard and Woodcock* [1957] and *Stramska et al.* [1990]. This parameter was not accounted for in the present study. However, the consequent application of the same experimental procedures, including the timing of the various steps, leads us to believe that the influence of this parameter will have been similar throughout all experiments and hence did not affect the results.

#### 4.1.3. Size Dependence

[24] The coefficient $a_j$ in equation (4), describing the temperature dependence of $\Phi_j$, is shown in Figure 8 as function of particle diameter $D_p$. At both the smaller and the larger ends of the particle range the values of $a_j$ show a clear trend. However, in the size range from 0.070 to 0.350 μm,

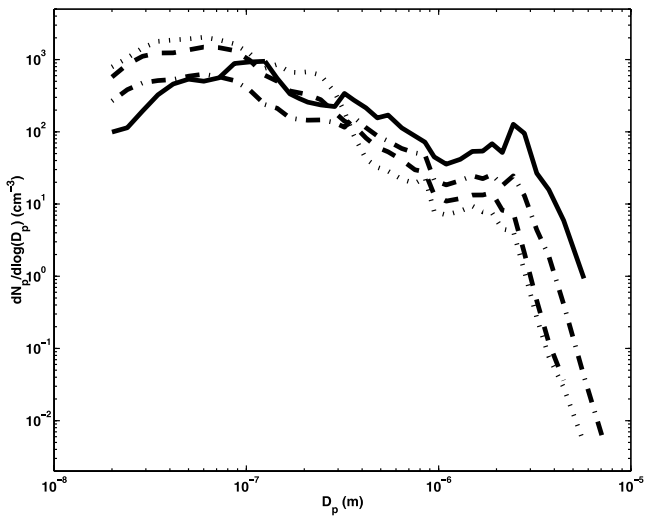


**Figure 6.** Number distributions of primary marine aerosol produced at water temperatures of −2°C (dotted line), 5°C (dashed line), 15°C (dot-dashed line), and 23°C (solid line) Here $q_b$ was 13 mL min$^{-1}$, and the salinity was 33‰.

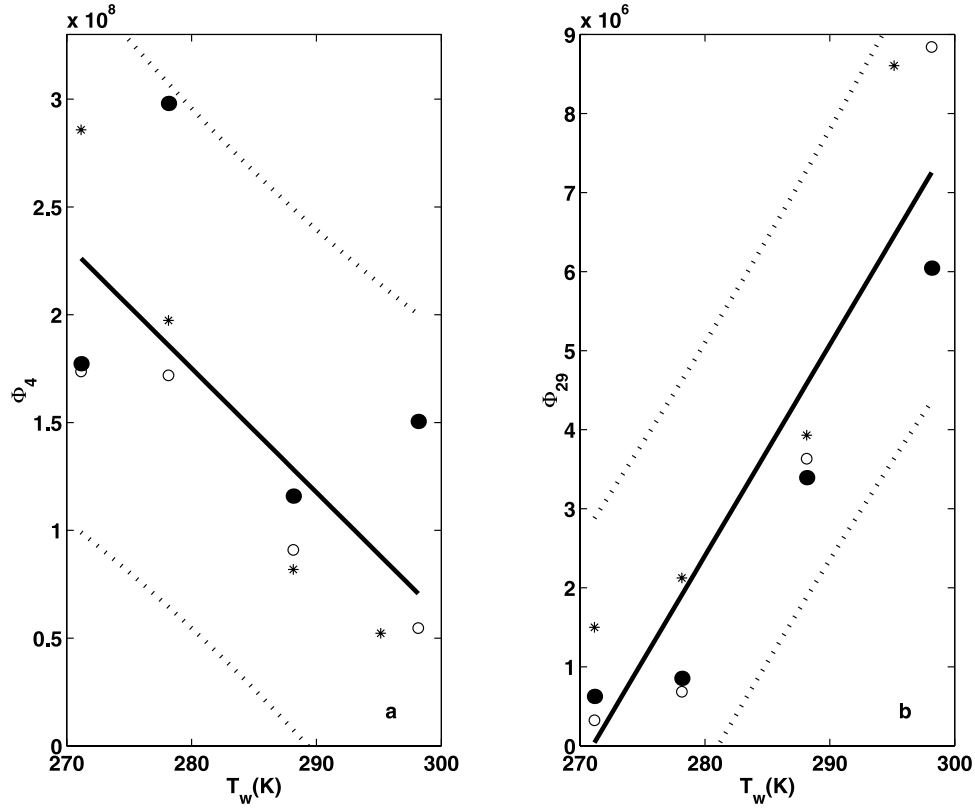


**Figure 7.** (a) The number of particles produced per second, logarithmic size increment, and water surface area with bubbles $\Phi_4$ which corresponds to the size class 0.0316 to 0.038 μm versus the temperature for three experiments with $q_b$ = 10 mL min$^{-1}$ (from two different measurements represented by open and closed circles) and $q_b$ = 13 mL min$^{-1}$ (stars). The salinity was 33‰. The curve is a linear fit, and the dashed lines correspond to a 95% confidence interval for the fit. (b) As Figure 7a, but for $\Phi_{29}$, which corresponds to the size class 1.4–1.6 μm.

$D_p$, there is no clear temperature dependence of the aerosol concentrations (compare Figure 6), and $a_j$ crosses zero 3 times in Figure 8. To describe the size dependence of $\Phi_j$, polynomials were fitted to the coefficients $a_j(D_p)$ and $b_j(D_p)$ in equation (4),

$$\left.\begin{aligned} A_k &= c_4 D_p^4 + c_3 D_p^3 + c_2 D_p^2 + c_1 D_p + c_0 \\ B_k &= d_4 D_p^4 + d_3 D_p^3 + d_2 D_p^2 + d_1 D_p + d_0 \end{aligned}\right\} \quad (5)$$

for three size intervals $k$: $k$ = 1, size ranges $j$ = 1–13 (0.020–0.145 μm); $k$ = 2, size ranges $j$ = 13–26 (0.145–0.419 μm); and $k$ = 3, size ranges $j$ = 26–38 (0.419–2.8 μm). The coefficients $c_l$ and $d_l$ ($l$ = 4–0) are presented in Table 1, and the fits to $a_j$ are graphically presented by the three curves in Figure 8. Depending on the water temperature, the parameterization can be used up to 2.8 μm, but to be sure it will not produce negative values, a break for this must be included in the parameterization. With these coefficients, equations (4) and (5) offer the required parameterization of $\Phi_j$ as a function of water temperature and dry aerosol size in a general form (independent of the choice of size intervals). The coefficients in Table 1 are given with four digits since the behavior of the polynomials in some size ranges is dependent on two terms of similar size but opposite sign.

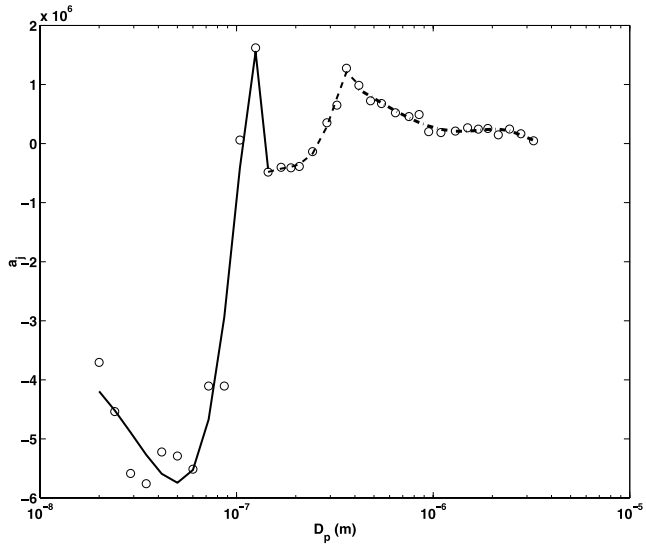


**Figure 8.** Coefficient $a_j$ (the first-order term in the fits between $\Phi_j$ and $T_w$) versus the diameter $D_p$ (circles). The curves are fourth-order polynomial fits which are applied in three diameter intervals: $D_p$ = 0.020–0.145 μm (solid line), $D_p$ = 0.145–0.419 μm (dashed line), and $D_p$ = 0.419–2.8 μm (dot-dashed line) (see text).

**Table 1.** Coefficients for the Parameterization of $A_k$ ($c_4$–$c_0$) and $B_k$ ($d_4$–$d_0$) in Equation (6) for the Three Size Intervals ($k$)

| Size Interval, $10^{-6}$ m | $c_4$ | $c_3$ | $c_2$ | $c_1$ | $c_0$ |
|---|---|---|---|---|---|
| 0.020–0.145 | $-2.576 \times 10^{35}$ | $5.932 \times 10^{28}$ | $-2.867 \times 10^{21}$ | $-3.003 \times 10^{13}$ | $-2.881 \times 10^{6}$ |
| 0.145–0.419 | $-2.452 \times 10^{33}$ | $2.404 \times 10^{27}$ | $-8.148 \times 10^{20}$ | $1.183 \times 10^{14}$ | $-6.743 \times 10^{6}$ |
| 0.419–2.8 | $1.085 \times 10^{29}$ | $-9.841 \times 10^{23}$ | $3.132 \times 10^{18}$ | $-4.165 \times 10^{12}$ | $2.181 \times 10^{6}$ |
| Size Interval, $10^{-6}$ m | $d_4$ | $d_3$ | $d_2$ | $d_1$ | $d_0$ |
| 0.020–0.145 | $7.188 \times 10^{37}$ | $-1.616 \times 10^{31}$ | $6.791 \times 10^{23}$ | $1.829 \times 10^{16}$ | $7.609 \times 10^{8}$ |
| 0.145–0.419 | $7.368 \times 10^{35}$ | $-7.310 \times 10^{29}$ | $2.528 \times 10^{23}$ | $-3.787 \times 10^{16}$ | $2.279 \times 10^{9}$ |
| 0.419–2.8 | $-2.859 \times 10^{31}$ | $2.601 \times 10^{26}$ | $-8.297 \times 10^{20}$ | $1.105 \times 10^{15}$ | $-5.800 \times 10^{8}$ |

[25] The resulting particle flux per whitecap area $F_p$ can now be estimated by combining equations (4) and (5) within each size range

$$\frac{dF_p}{d\log D_p} = \Phi = A_k T_w + B_k \tag{6}$$

Equation (6) is able to reproduce the original measurements fairly well considering the variability in the data except for the small concentrations at the largest sizes at $T_w < 0°C$, for which the parameterization produces too small or negative values. Figure 9 shows a comparison between $\Phi_{\text{fit}}$ from equation (6) and $\Phi$ representing all data points presented in Figure 3. For most of the sizes and temperatures the fits differ less then a factor 2 from the measurements.

### 4.2. Comparison With Field Measurements and Other Flux Parameterizations

#### 4.2.1. Total Number Fluxes

[26] Combining equation (6) with the whitecap cover equation (2), an expression results for the total particle flux $F_0$ from the ocean,

$$\frac{dF_0}{d\log D_p} = \Phi W \tag{7}$$

With this approach the problem of defining the primary marine aerosol source flux through the ocean surface has been broken down into two parts: the whitecap cover and the particle production per whitecap surface area and size increment. It is assumed that these are independent of each other. *Nilsson et al.* [2001] measured the primary marine aerosol source flux through the surface layer, with an eddy covariance flux system. Therefore the measured flux is an average over a relatively large area, with both whitecaps and clear water. In the parameterized flux in equation (7) this is accounted for by the fraction of whitecap cover. It is worth mentioning that among the various versions of equation (2) in literature this is the one that has the most similar slope to the flux measurements by *Nilsson et al.* [2001] in Figure 10.

[27] The applicability of our parameterization at water temperatures below 0°C is not straightforward because in practice such water temperatures will occur only in the leads between ice floes in the Arctic and Antarctic waters. Over the leads the fetch of the open water is usually so small that whitecaps form only at wind speeds >20 m $s^{-1}$. Hence the usual parameterization of the whitecap cover as function of wind speed [*Monahan and O'Muircheartaigh*, 1980] (equation (2)) cannot be used for the leads. Following *Nilsson et al.* [2001], the primary marine aerosol flux in this condition is reduced by an order of magnitude.

[28] The source function thus derived (equation (7)) is referred to as MN02 and is plotted in Figure 10, together with the one derived from the direct measurements (equation (1)) of *Nilsson et al.* [2001] and the two most commonly used source functions [*Monahan et al.*, 1986; *Smith et al.*, 1993] and the one from *Cipriano et al.* [1987]. Considering the total aerosol number based on laboratory experiments, MN02 compares favorably with *Nilsson et al.* [2001]. The source function from *Monahan et al.* [1986] (referred to as MH86) is given by

$$\frac{dF_0}{dr} = 1.373 U_{10}^{3.41} r^{-3} \left(1 + 0.057 r^{1.05}\right) \times 10^{1.19 e^{-B^2}} \tag{8}$$

in $m^{-2}$ $s^{-1}$ $\mu m^{-1}$, where $B = (0.380 - \log r)/0.650$ and $r$ is the radius at a relative humidity of 80%. MH86 is valid in the size range 0.8–10 μm $r$ (corresponding to 0.9–11.4 μm $D_p$).

[29] The total source flux derived by *Smith et al.* [1993] (hereinafter referred to as SM93) is formulated as the sum of two lognormal distributions and is valid in the size range 1–25 μm $r_{80}$, the particle radius at 80% relative humidity (1.1–28 μm $D_p$),

$$\frac{dF_0}{dr_{80}} = \sum_{i=1,2} A_i \exp\left[-f_i \left(\ln \frac{r_{80}}{r_{0i}}\right)^2\right] \tag{9}$$

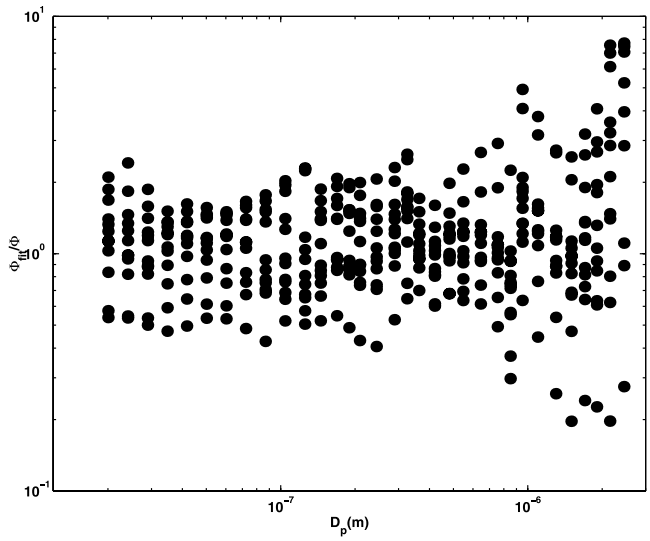


**Figure 9.** The ratio of the parameterized $\Phi_{fit}$ and all experimental data points $\Phi$ over different aerosol dry diameters.

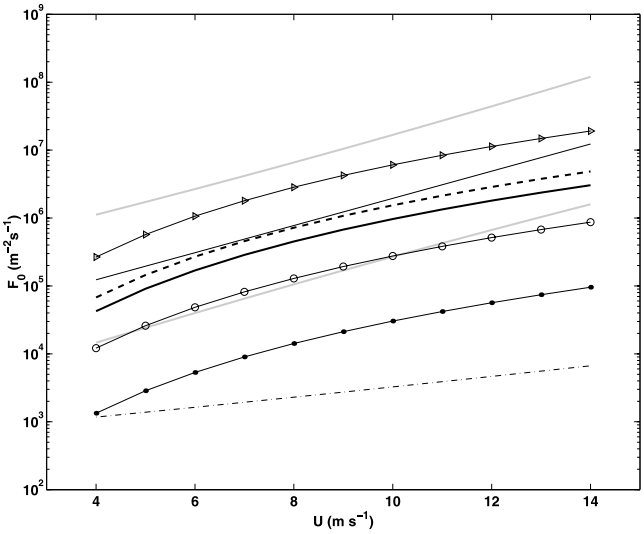


**Figure 10.** Comparison of total number flux parameterizations $F_0$ as function of the wind speed $U$. The source flux of the primary marine aerosol from equation (7) for two different temperatures 25°C $T_w$ (solid bold line) and 5°C $T_w$ (dashed line) are compared to the in situ total primary marine aerosol source flux measured by *Nilsson et al.* [2001] (solid line). The shaded lines represent the 99% confidence interval of the best fit to *Nilsson et al.* [2001]. Also plotted is the flux from *Monahan et al.* [1986] in the size interval 0.9–11.2 μm $D_p$ (line with dots) and extrapolated down to 0.02 μm, i.e., within a total size interval 0.02–11.2 μm $D_p$ (line with triangles), and the flux derived by *Smith et al.* [1993] (dot-dashed line) and *Cipriano et al.* [1987] (line with circles).

in m$^{-2}$ s$^{-1}$ μm$^{-1}$. The constants $f_1$, $f_2$, $r_{01}$, and $r_{02}$ have the values 3.1, 3.3, 2.1, and 9.2 μm, respectively. The coefficients $A_1$ and $A_2$ depend on the wind speed

$$\left.\begin{aligned}\log(A_1) &= 0.0676U + 2.43\\ \log(A_2) &= 0.959U^{1/2} - 1.476\end{aligned}\right\} \quad (10)$$

MH86 integrated over the valid size interval 0.9–11.2 μm $D_p$ is much smaller than the total source flux MN02, because the large contribution by particles smaller than 0.9 μm $D_p$ is not included. If MH86 is extrapolated down to 0.020 μm $D_p$, the total integrated number flux is instead larger than MN02 and the *Nilsson et al.* [2001] field measurements; see discussion below. Also, SM93 estimates the flux only for particles with $D_p > 1.1$ μm, so the total fluxes are small in comparison with those derived here. *Cipriano et al.* [1987] combined the flux of particles per whitecap area $F_p = 2.8 \times 10^7 \pm 0.9$ m$^{-2}$ s$^{-1}$ with $W$ (equation (2)), which resulted in a total particle flux, $F_0$; the size interval is not defined, but it also contains submicron particles.

#### 4.2.2. Size-Resolved Fluxes

[30] In Figure 11 the different parameterizations are compared for a wind speed of 9.0 m s$^{-1}$. The expressions for the source fluxes have been converted to $dF_0/d\log D_p$ (m$^{-2}$ s$^{-1}$), where $D_p$ is the dry diameter. MN02 describes the aerosol flux down to $D_p$ = 0.020 μm, with modes centered at ~0.07 μm and 2 μm $D_p$. The magnitude of the flux depends on the water temperature. Below $D_p$ = 0.1 μm the number flux is higher for the cold water as derived from the experimental data in Figure 6. Above 0.2 μm $D_p$ the number flux is higher for the warm water.

[31] In large-scale models, MH86 has been extrapolated beyond its range of validity [e.g., *Gong et al.*, 1997; *Lohmann et al.*, 2000]. Figure 11 shows that the extrapolated MH86 flux increases monotonously with decreasing $D_p$ below 0.9 μm, and as expected, the size spectra observed in the laboratory study as well in the field measurements (compare Figure 4) are not reproduced. In the size range $D_p$ = 0.07–0.9 μm, MH86 may underestimate the flux, and below 0.07 μm $D_p$, MH86 overestimates the flux, compared to MN02. The failure of the MH86 approach below 1 μm $D_p$ is because it is based on a simple power law fit to an aerosol mode located at ~1 μm $D_p$ [*Monahan et al.*, 1986, Figure 4]. Hence this parameterization is too simple to reproduce the observed properties. The underestimation in the 0.07–0.9 μm $D_p$ range and the overestimation in the $D_p < 0.07$ μm partly cancel when the total number flux is determined; see Figure 10. However, the shift of aerosol number from above to below 0.9 μm $D_p$ may make a significant difference if one considers the contribution of the primary marine aerosol source to the cloud condensation nuclei (CCN) population. In any case, the MN02 parameterization should be preferred in the $D_p < 0.9$ μm range since this is outside the range of the experimental data on which MH86 is based. In the supersaturation expected in, for example, marine stratus, sea-salt particles $D_p > 0.08$ μm would be activated as CCN. Hence MN86 is likely to result in lower CCN production

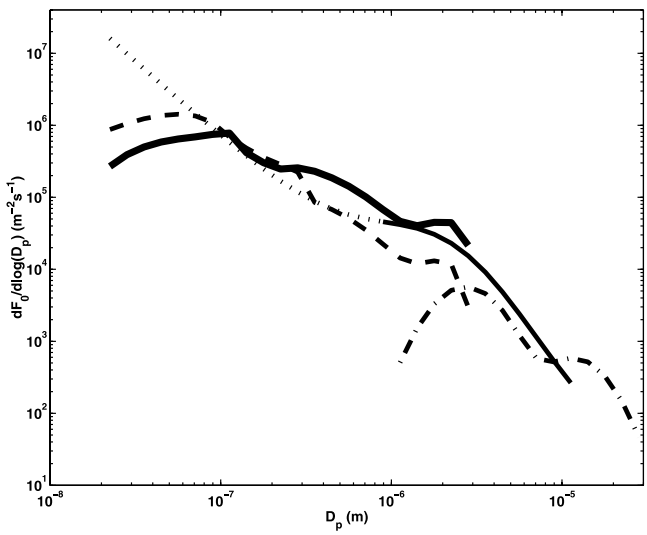


**Figure 11.** Comparison with other source flux parameterizations, $dF_0/d\log D_p$, as functions of the dry particle diameter $D_p$, for a wind speed of 9 m s$^{-1}$. The source flux MN02 derived in this paper is plotted for water temperatures of 25°C $T_w$ (solid bold line) and 5°C $T_w$ (dashed line). These results are compared with the source flux from *Monahan et al.* [1986] in the size interval 0.9 – 11.2 $D_p$ μm (solid line) and extrapolated down to 0.02 μm, i.e., in the size interval 0.020–0.9 μm $D_p$ (dotted line), and the flux derived by *Smith et al.* [1993] (dot-dashed line).

than MN02 and thus in different cloud properties and radiative forcing. For $D_p$ = 0.9–3.0 μm, MN02 and MH86 agree fairly well. MH86 did not report the temperature of the experiment, but the two source functions agree best for 15°C (not shown). For $D_p$ > 3.0 μm, MN02 seems to underestimate the source flux compared both to MH86 and SM93.

## 5. Summary and Conclusions

[32] In all its simplicity our experimental setup has provided the possibility of studying the aerosol spectra produced by bubble bursting. We have been able to measure the size distribution of the simulated primary marine aerosol particles and found a contribution down to 0.020 μm $D_p$ (dry diameter). This lower size cut is smaller than in any previous laboratory experiment, thereby covering the gap between previous laboratory experiments (and parameterizations) and more recent field measurements. All aerosol number size spectra in Figures 3–6 show a major contribution of particles in the submicrometer range. We can distinguish a minimum in all size spectra at $D_p$ = 1 μm, which separates a mode at ~0.1 μm and another one at ~2.5 μm. *O'Dowd and Smith* [1993] discerned a film drop number concentration mode ($D_p \approx 0.2$ μm) and a jet drop mode ($D_p \approx 2$ μm) from measurements over the northeast Atlantic. *Nilsson et al.* [2001] found modes centered at 0.1 μm and 1–2 μm, respectively. In remote marine air, *Murphy et al.* [1998] showed that although the sea-salt mass fraction of the aerosol was larger at larger sizes, about half the mass near 100 nm $D_p$ was sea salt. These field measurements are in favorable agreement with the presented laboratory results. To our knowledge, the only previous laboratory experiment that has presented an aerosol number size distribution down to this size range is from *Resch and Afeti* [1992], but it is for larger bubbles (2.14 mm $D_b$). The temperature dependence of the number concentrations in the current experiments is qualitatively similar to that observed by *Bowyer et al.* [1990]. No explanation is currently offered for the reasons for the temperature dependence, which would require additional research into this phenomenon. However, the changes in the aerosol number distributions as functions of water temperature and salinity indicate different formation processes for small and large droplets.

[33] There is qualitative and quantitative agreement between our parameterization and the measurements by *Nilsson et al.* [2001]. This is an indication for the validity of equations (4), (5), and (7) as a practical formulation of the sea spray source function, although of course more comparisons are required with experimental data to arrive at a universal source function. Also, the precision in the presently available eddy covariance aerosol fluxes would not be enough to confirm the parameterization to within better than an order of magnitude.

[34] The total aerosol number source flux we have derived is rather large compared to previous parameterizations because we have extended the size range and found most of the aerosol production in the submicrometer size range, far below the valid size range of previous parameterizations. Our number source flux is, however, smaller than that from the parameterization by *Monahan et al.* [1986] if this is extrapolated to similar sizes (below its range of validity). This has consequences for the number flux in the 0.07–0.9 μm $D_p$ range and hence for the CCN formation from the primary marine aerosol. For example, at a sea surface temperature of 2°C, a wind speed of 10 m $s^{-1}$, and a mixed layer depth of 500 m, on the basis of MN02 parameterization, 282 new particles per cubic centimeter would be produced in 1 day. Obviously, the resulting number concentration would be smaller because of sink processes, but considering that the marine boundary layer often has an aerosol number concentration of a few hundred particles per cubic centimeter, the contribution from the primary marine aerosol source should be significant, especially for the CCN fraction of the aerosol.

[35] If the oceans would warm as a result of the increasing amount of anthropogenic greenhouse gases in the atmosphere, the primary marine aerosol flux would change in magnitude, and the size spectra would change. In regions where the water temperature increases, the number of small particles would decrease, and the concentrations of large ones would increase. The supersaturation in the marine clouds and the competition by other aerosol sources will determine what fraction of the particles will be activated. In most marine clouds, sea-salt particles down to ~0.08 μm $D_p$ would be activated. A climate warming would therefore probably increase the primary marine aerosol contribution to the CCN, resulting in a negative feedback. From the differences between the parameterized fluxes from the present study at different temperatures as seen in Figures 10 and 11, it can be concluded that temperature changes are likely to cause smaller changes in the primary marine aerosol source than a small change in the wind speed would. An increasing wind speed is expected as a result of global warming, which could then increase the CCN concentration and the cloud albedo, and this could result in a negative feedback.

[36] **Acknowledgments.** We would like to acknowledge the Swedish Natural Science Research Council (contracts G-AA/AS 11858-302, G-AA/GU 11858-303 and G 5103-20005689) for financial support. TNO research in the field of marine aerosols is financially supported by the Netherlands Ministry of Defence (several projects) and the U.S. Office of Naval Research, grant N00014-96-1-0581.

## References

Aitken, J., On dust, fogs, and clouds, *Trans. R. Soc., Edinburgh*, *30*, 337–368, 1881.

Andreas, E. L., A new spray generation function for wind speeds up to 32 m $s^{-1}$, *J. Phys. Oceanogr.*, *34*, 77–95, 1998.

Blanchard, D. C., The electrification of the atmosphere by particles from bubbles in the sea, *Prog. Oceanogr.*, *1*, 71–202, 1963.

Blanchard, D. C., The production, distribution and bacterial enrichment of the sea-salt aerosol, in *The Air-Sea Exchanges of Gases and Particles*, edited by P. S. Liss and W. G. N. Slinn, pp. 407–454, D. Reidel, Norwell, Mass., 1983.

Blanchard, D. C., and L. D. Sydzek, Film-drop production as a function of bubble size, *J. Geophys. Res.*, *93*, 3649–3654, 1988.

Blanchard, D. C., and A. H. Woodcock, Bubble formation and modification in the sea and its meteorological significance, *Tellus*, *9*, 145–158, 1957.

Bortkovskii, R. S., *Heat and Moisture Exchange Between Atmosphere and Ocean Under Storm Conditions*, 160 pp., Hydrometeorol. Publ., Leningrad, Russia, 1983.

Bowyer, P. A., Video measurements of near-surface bubble spectra, *J. Geophys. Res.*, *106*, 14,179–14,190, 2001.

Bowyer, P. A., D. K. Woolf, and E. C. Monahan, Temperature dependence of the charge and aerosol production associated with a breaking wave in a whitecap simulation tank, *J. Geophys. Res.*, *95*, 5313–5319, 1990.

Cipriano, R. J., E. C. Monahan, P. A. Bowyer, and D. K. Woolf, Marine condensation nucleus generation inferred from whitecap simulation tank results, *J. Geophys Res.*, *92*, 6569–6576, 1987.

De Leeuw, G., F. P. Neele, M. Hill, M. H. Smith, and E. Vignati, Sea spray aerosol production by waves breaking in the surf zone, *J. Geophys. Res.*, *105*, 29,397–29,409, 2000.

Gong, S. L., L. A. Barrie, and J.-P. Blanchet, Modeling sea-salt aerosols in the atmosphere: 1, Model development, *J. Geophys. Res.*, *102*, 3805–3818, 1997.

Leifer, I., G. de Leeuw, and L. H. Cohen, Secondary bubble production from breaking waves: The bubble burst mechanism, *Geophys. Res. Lett.*, *27*, 4077–4080, 2000.

Leifer, I., G. de Leeuw, and L. H. Cohen, Optical measurement of bubbles: System design, *J. Atmos. Oceanic Technol.*, in press, 2002.

Lohmann, U., J. Feichter, J. Penner, and R. Leaitch, Indirect effect of sulfate and carbonaceous aerosols: A mechanistic treatment, *J. Geophys. Res.*, *105*, 12,193–12,206, 2000.

Medwin, H., and N. D. Breitz, Ambient and transient bubble spectral densities in quiescent seas and under spilling breakers, *J. Geophys. Res.*, *94*, 12,751–12,759, 1989.

Monahan, E. C., and I. O'Muircheartaigh, Optimal power-law description of oceanic whitecap coverage dependence on wind speed, *J. Phys. Oceanogr.*, *10*, 2094–2099, 1980.

Monahan, E. C., C. W. Fairall, K. L. Davidson, and P. J. Boyle, Observed inter-relations between 10 m winds, ocean whitecaps and marine aerosols, *Q. J. R. Meteorol. Soc.*, *109*, 379–392, 1983.

Monahan, E. C., D. E. Spiel, and K. L. Davidson, A model of marine aerosol generation via whitecaps and wave disruption, in *Oceanic Whitecaps*, edited by E. C. Monahan and G. MacNiochaill, pp. 167–193, D. Reidel, Norwell, Mass., 1986.

Murphy, D. M., J. R. Anderson, P. K. Quinn, L. M. McInnes, F. J. Brechtelk, S. M. Kreidenweisk, A. M. Middlebrook, M. Po'sfai, D. S. Thomson, and P. R. Buseck, Influence of sea-salt on aerosol radiative properties in the Southern Ocean marine boundary layer, *Nature*, *392*, 62–65, 1998.

Nilsson, E. D., Ü. Rannik, E. Swietlicki, C. Leck, P. P. Aalto, J. Zhou, and M. Norman, Turbulent aerosol fluxes over the Arctic Ocean: 2. Wind-driven sources from the sea, *J. Geophys. Res.*, *106*, 32,111–32,124, 2001.

O'Dowd, C. D., and M. H. Smith, Physiochemical properties of aerosols over the northeast Atlantic: Evidence for wind-related submicron sea-salt aerosol production, *J. Geophys. Res.*, *98*, 1137–1149, 1993.

O'Dowd, C. D., M. H. Smith, I. E. Consterdine, and J. A. Lowe, Marine aerosol, sea-salt, and the marine sulphur cycle: A short review, *Atmos. Environ.*, *31*, 73–80, 1997.

Resch, F. R., and G. Afeti, Submicron film drop production by bubbles in seawater, *J. Geophys. Res.*, *97*, 3679–3683, 1992.

Smith, M. H., P. M. Park, and I. E. Consterdine, Marine aerosol concentrations and estimated fluxes over the sea, *Q. J. R. Meteorol. Soc.*, *119*, 809–824, 1993.

Spiel, D. E., The number and size of jet drops produced by air bubbles bursting on a fresh water surface, *J. Geophys. Res.*, *99*, 10,289–10,296, 1994.

Spiel, D. E., More on the births of jet drops from bubbles bursting on seawater surfaces, *J. Geophys. Res.*, *102*, 5815–5821, 1997a.

Spiel, D. E., A hypothesis concerning the peak in film drop production as a function of bubble size, *J. Geophys. Res.*, *102*, 1153–1161, 1997b.

Spiel, D. E., On the birth of film drops from bubbles bursting on seawater surfaces, *J. Geophys. Res.*, *103*, 24,907–24,918, 1998.

Stramska, M., R. Marks, and E. C. Monahan, Bubble-mediated aerosol production as a consequence of wave breaking in supersaturated (hyperoxic) seawater, *J. Geophys. Res.*, *95*, 18,281–18,288, 1990.

Woodcock, A. H., Salt nuclei in marine air as a function of attitude and wind force, *J. Meteorol.*, *10*, 362–371, 1953.

Woolf, D. K., P. A. Boywer, and E. C. Monahan, Discriminating between the film drops and jet drops produced by a simulated whitecap, *J. Geophys. Res.*, *92*, 5142–5150, 1987.

L. H. Cohen and G. de Leeuw, TNO Physics and Electronics Laboratory, P.O. Box 96864, 2509 JG The Hague, Netherlands. (cohen@fel.tno.nl; deleeuw@fel.tno.nl)

H.-C. Hansson, Air Pollution Laboratory, ITM, Stockholm University, SE-10691 Stockholm, Sweden. (HC@itm.su.se)

E. M. Mårtensson and E. D. Nilsson, Department of Meteorology, Stockholm University, Stockholm, Sweden. (monica@misu.su.se; dolan@misu.su.se)